A. Data Preparation

Time series data The time series data for the variables pressure, vibration and temperature, along with the electrodes data are visualised (Appendix A, Figure 6 to Figure 13). A time step is chosen to allow differentiation between the data for different objects by considering at each time step i: (i) the inter-object variance A, (ii) the smallest squared distance between two objects B, and (iii) the intra-object variance C. A score is then generated for each time step i according to the equation $\text{Score}_i = 0.35A_i + 0.45B_i - 0.2C_i$. The score increases as the inter-object variance and the smallest squared distance between two object increases, and it decreases as the intra-object variance increases. The time step with the highest score was then chosen for sampling of the data ($i = 38$). This time step also has a physical significance as it is likely to be the time at which the finger grippers made early contact with the objects. Thus, meaningful data about the physical properties of the objects such as hardness and texture can be obtained.

Scatter plot of the PVT data The time series data is sampled at the time step $i = 38$. A 3D scatter plot is then generated based on the sampled time series data for the six objects (Appendix A, Figure 14).

B. Principal Component Analysis

Covariance matrix, eigenvalues and eigenvectors The covariance matrix S, eigenvalues λ and eigenvectors v for the standardised PVT data are reported below.

$$S = \begin{bmatrix} 1 & -0.4170 & 0.2805 \\ -0.4170 & 1 & -0.3095 \\ 0.2805 & -0.3095 & 1 \end{bmatrix} \tag{1}$$

$$\lambda_1 = 1.6750, \quad \lambda_2 = 0.7440, \quad \lambda_3 = 0.5810 \tag{2}$$

$$v_1 = \begin{bmatrix} 0.5944 \\ -0.6084 \\ 0.5259 \end{bmatrix}, \; v_2 = \begin{bmatrix} -0.4465 \\ 0.2943 \\ 0.8450 \end{bmatrix}, \; v_3 = \begin{bmatrix} 0.6688 \\ 0.7371 \\ 0.0967 \end{bmatrix} \tag{3}$$

Plot of standardised data with principal components The principal components are the eigenvectors that resulted in the largest variances (eigenvalues) between the data points when projected onto that component (Figure 1).

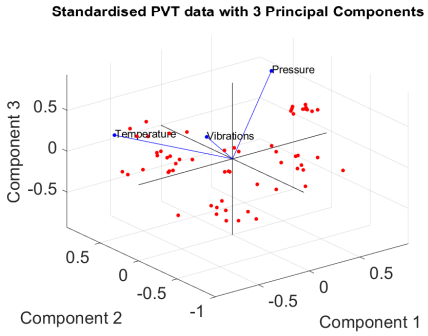

Figure 1: Standardised PVT data with 3 principal components

Reducing data to 2 dimensions The principal components associated with the 2 largest eigenvalues are used to reduce the data to 2 dimensions (Appendix, Figure 16).

Distribution of data along the principal components As the eigenvalue of the associated eigenvector decreases, the variance of points along the eigenvector decreases. However, since the variance between the three princpial components are similar (Figure 2), it is difficult to justify reducing the dimensions of the PVT data.

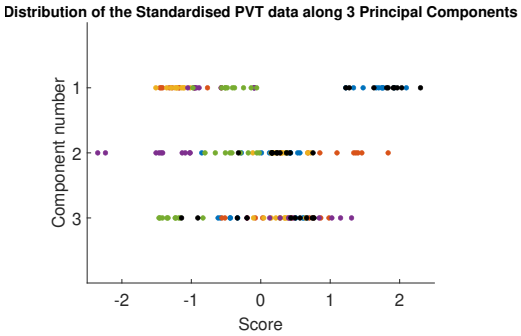

Figure 2: Distribution of the standardised data along the principal components

Conclusion None of the three principal components seem to be redundant since their variances are similar. In other words, none of the principal components heavily outweigh the others in the amount of information stored. This is not very surprising because the PVT data is only three-dimensional, and contains measurements of very different physical properties which do not have large covariances. PCA would be more useful for data with a higher number of dimensions.

Principal components of electrode data The variance of each principal component is shown in a Scree plot (Fig-

ure 3).

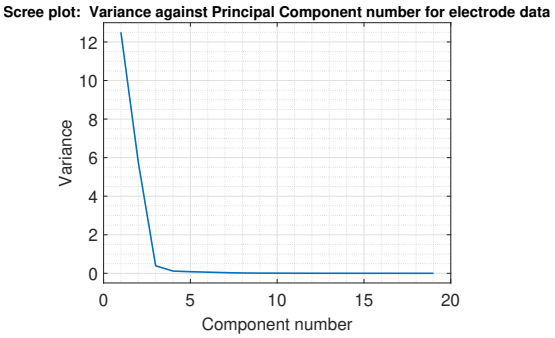

Figure 3: Variance against principal component number for electrode data

There is a sharp decrease in the variance from component number 1 to component number 3. Furthermore, the gradient of the scree plot becomes shallow after the third principal component which suggests that the amount of information stored in component numbers 3 to 19 are similar. Thus, the data can be reduced from 19 dimensions to 3 dimensions. The electrode data is also projected onto each of the 19 principal components to obtain another representation of how the variance evolves over component number (Appendix B, Figure 20). After the third principal component, the variance of the electrode data becomes small.

Dimensionality reduction of electrodes data The electrodes data is reduced to be three dimensional using the three principal components with the largest variances (Appendix B, Figure 19).

Conclusion The electrode data had 19 dimensions, however, the dimensions were not all equally informative. Performing PCA allowed for dimensionality reduction by first identifying the principal components, and then retaining only the principal components with the largest variances, with little information lost.

C. Linear Discriminant Analysis

Using LDA to split the 2D PVT data of the black foam and the car sponge LDA is applied to all 2D feature space combinations of the PVT data (i.e. Pressure vs Vibration, Pressure vs Temperature, and Temperature vs Vibration). The LD function was then found which maximised inter-class separability, while minimising the intra-class variance (Appendix C, Figure 21 to Figure 23). The plot of the projection of data onto the LD function demonstrates that the classes are well separated (Figure 4).

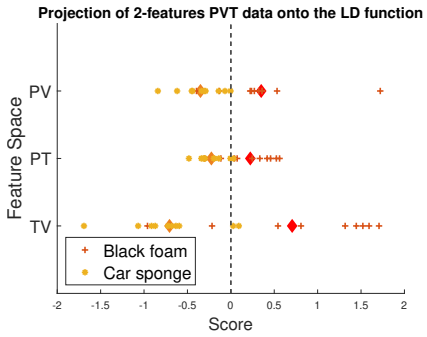

Figure 4: Projection of the black foam and car sponge PVT data onto the LD functions associated with the 2D feature space defined by the y-axis (e.g. PV: pressure and vibrations feature space). The mean of the standardised data is zero, and the means of the individual classes are represented by diamonds.

Applying LDA to 3D PVT data of the black foam and the car sponge The two LD axis which resulted in the best separation of the classes are plotted (Figure 5, LD1 and LD2: green and blue lines respectively).

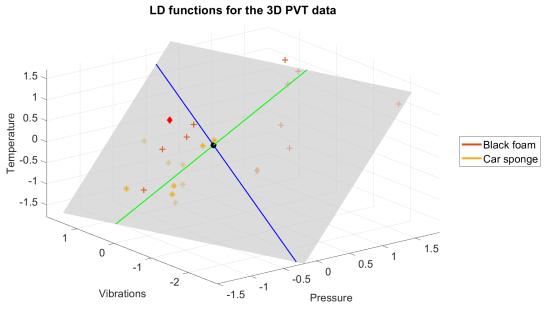

Figure 5: Two LD functions (green and blue) with the best separation for the black foam and car sponge 3D PVT data. The plane defined by the two LD functions is shown in gray.

Comment on results The black foam and car sponge are not good conductors of heat, are easily deformable, and have similar textures which leads to close temperature, pressure and vibrations readings respectively. Since they have similar physical properties, it can be difficult to perfectly classify data into one of the two classes. However, the two objects differ most in terms of pressure and temperature, which allows for classification based primarily on these two features. Thus, unsurprisingly, the LD function based on the PT feature space resulted in the best separation (Appendix C, Figure 22), as determined by the eigenvalues. Additionally, the LD1 function generated from the 3D PVT data has better separation than the 2D PT data due to the additional degree of freedom.

LDA analysis on the flour sack and kitchen sponge (Appendix C, Figure 28 to Figure 34) The flour sack and kitchen sponge are similar because they are bad conductors of heat and are deformable. However, the flour sack is softer than the kitchen sponge, and the texture of the two objects are different, since one side of the kitchen sponge is rough. Based on these characteristics of the objects, two hypotheses were made: (i) LDA of the 3D PVT data of the flour sack and kitchen sponge will have better separation than for the black foam and car sponge as determined by the eigenvalues, and (ii) the LD function generated from the PV feature space data will result in the best separation among the other 2D feature spaces.

The first hypothesis was correct, since the eigenvalue of the LD1 function for the flour sack and kitchen sponge PVT data was larger than the black foam and kitchen sponge ($2.2523 > 0.2237$). However, the second hypothesis was wrong. The eigenvalue of the LD function associated with the TV feature space is larger than the PV feature space ($2.1365 > 1.7867$).

D. Clustering

Clustering of the PVT data Hierarchical clustering using the distance metrics "standardised euclidean" (seuclidean) and "mahalanobis" were performed (Appendix D, Figure 36 and Figure 38 respectively). Both distance metrics grouped acrylic and steel vase data points into one cluster. This is likely because both objects are hard and smooth and thus, have similar pressure and vibrations readings. Additionally, the seuclidean metric grouped all the black foam and car sponge data points into one cluster due to their similar physical properties as discussed. The mahalanobis metric resulted in more equally sized clusters, and even perfectly grouped all the flour sack data into one cluster.

Bagging of the three-dimensional electrode data The number of trees to use was considered a hyperparameter and it was tuned. The space from 1 to 100 trees were explored using 10 rng seeds, and the maximum test accuracy was obtained when 18 trees were used (Appendix D, Figure 39). Two of the trees in the ensemble are also visualised (Appendix D, Figure 41 and 42). The overall test accuracy of the ensemble of trees is high at 95.83% since it only misclassified one steel vase data point as acrylic (confusion matrix; Appendix D, Figure 43). This is likely because both objects are smooth and hard.

Applying PCA to the electrodes data reduced the dimensions from 19 to 3. This reduced the computational complexity of the classification problem. Most of the important information is kept in the three largest principal components, which is why the classification accuracy is still high. However, in the process of dimensionality reduction, some information was lost which contributed to why the classifier was not perfect. Since the choice to reduce the dimensions to 3 is subjective, it can also be argued that a reduction of dimensionality to 4 would lead to a higher classification accuracy.

E. Conclusions

PCA has helped in the identification of principal components that are most informative. LDA helped in the classification of data points by generating a function which maximises the separation between classes. Clustering groups the data points by proximity which can reveal objects that have similar physical properties. Finally, bagging allowed for better classification generalisation by combining the results of multiple trees.

If the objects have very different physical properties, such as the steel vase and kitchen sponge, then touch alone can be robust enough to differentiate the two objects. However, for objects with more similar physical properties such as the black foam and car sponge, it might be challenging for touch alone to perfectly distinguish the objects.

The choice of sensors and properties to measure depends on the objects of interest. However, for the six objects analysed in this report, PCA revealed that pressure has the lowest variance and is thus, slightly less informative than the temperature and vibrations data. Additionally, PCA also revealed that fewer electrodes can be used. In order to obtain a more definitive answer, Lasso regularisation can be used during classification to determine the features that are least important.

Finally, there are other ways to prepare the data before analysis. The PVT data in this report has three features since the data was sampled at a single time step. In theory, the entire time series data can be used as the feature space, however, this has a large computational burden. Instead, the time series data can be sampled at multiple time steps, for instance 10, to obtain PVT data that has 30 features.

Appendix

Appendix A

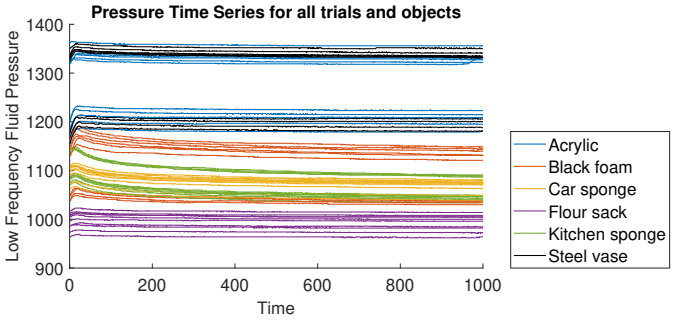

Figure 6: Pressure time series data for all trials and objects

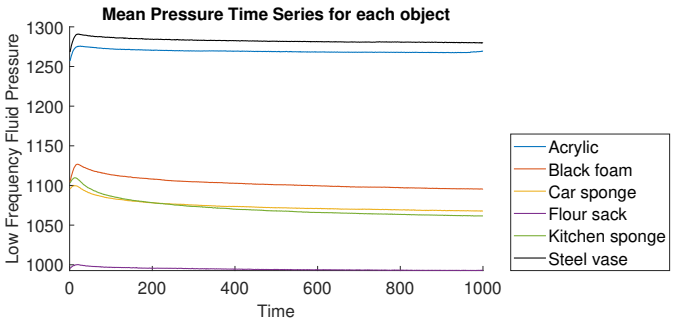

Figure 7: Mean pressure time series data for each object

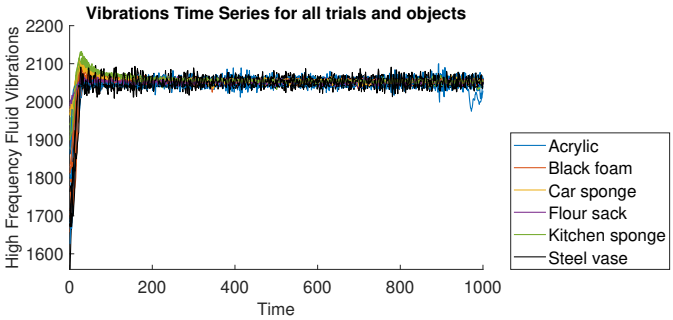

Figure 8: Vibrations time series data for all trials and objects

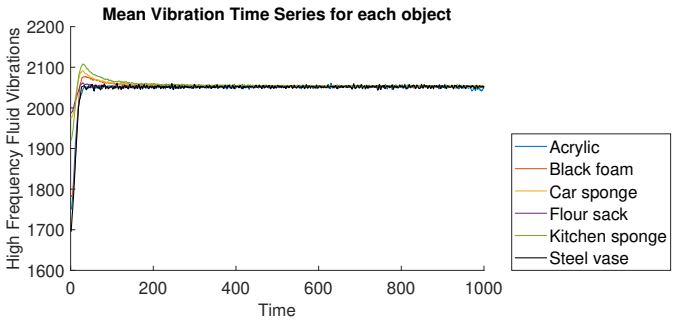

Figure 9: Mean vibrations time series data for each object

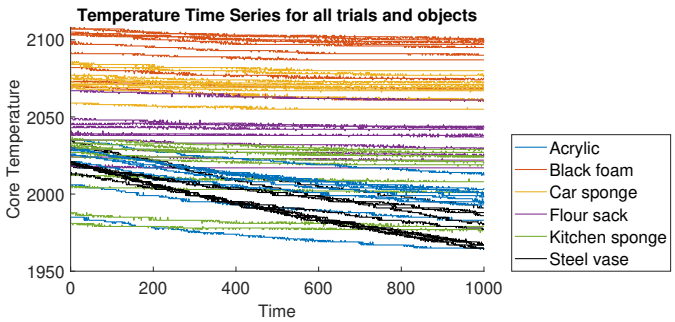

Figure 10: Temperature time series data for all trials and objects

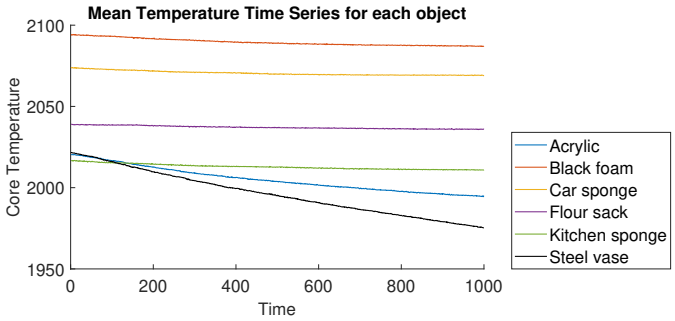

Figure 11: Mean temperature time series data for each object

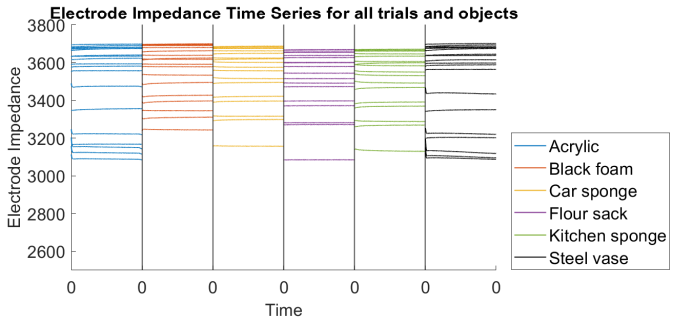

Figure 12: Electrode impedance time series data for all trials and objects. Note that the x-axes for the different objects have been merged into one. For each object, the electrode impedance data starts from $t = 0$ and ends at $t = 1000$.

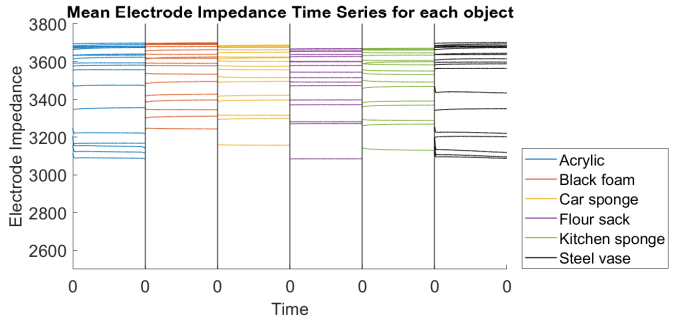

Figure 13: Mean electrode impedance time series data for each object. Note that the x-axes for the different objects have been merged into one. For each object, the electrode impedance data starts from $t = 0$ and ends at $t = 1000$.

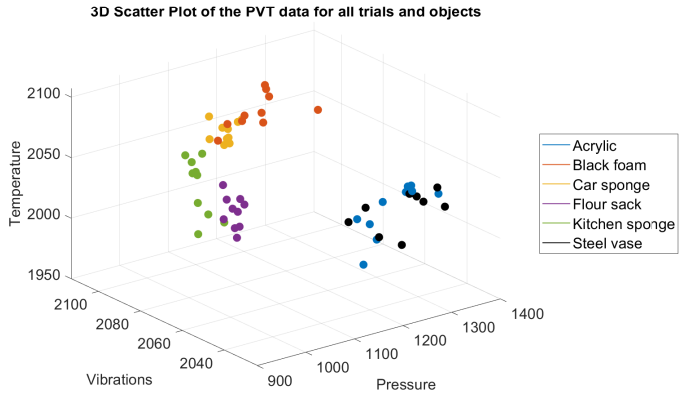

Figure 14: 3D scatter plot of the PVT data for all trials and objects

Appendix B

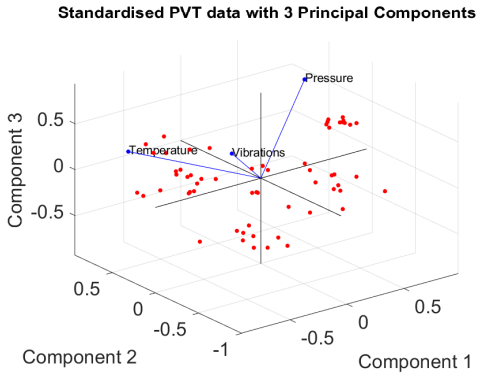

Figure 15: Standardised PVT data with three principal components

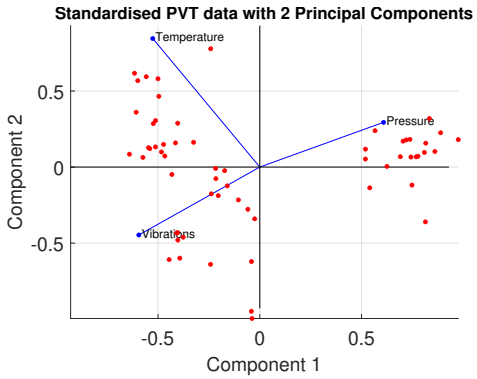

Figure 16: Standardised PVT data with two principal components

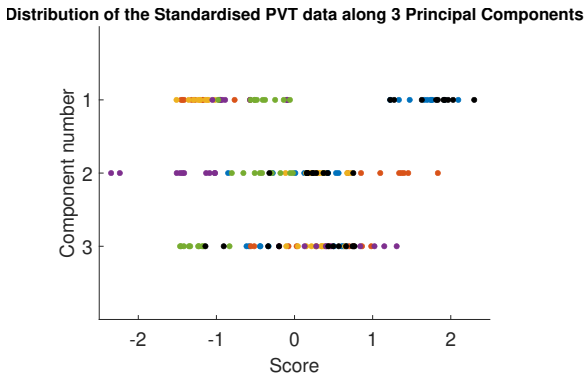

Figure 17: Distribution of the standardised PVT data along three principal components

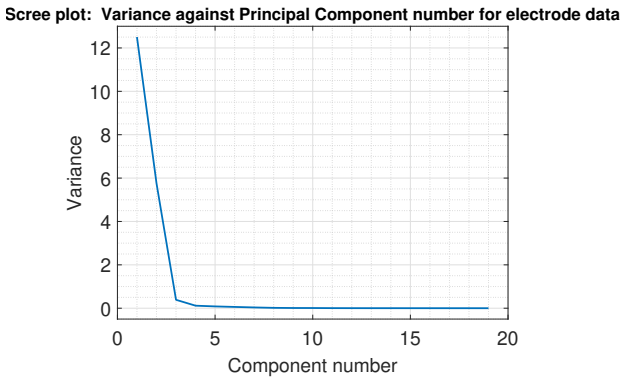

Figure 18: Scree plot: Variance against principal component number for electrode data

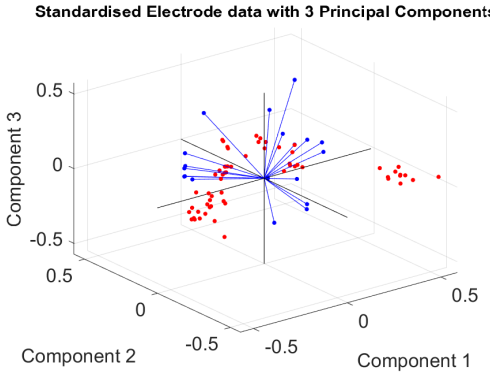

Figure 19: Standardised electrode data with three principal components

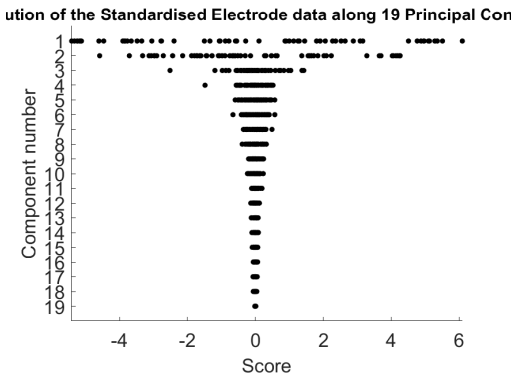

Figure 20: Distribution of the standardised electrode data along 19 principal components

Appendix C

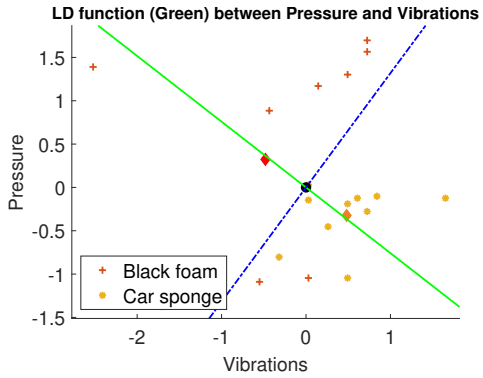

Figure 21: LD function (green) for the pressure and vibrations feature space of the black foam and car sponge. The separating hyperplane (line) is shown in blue.

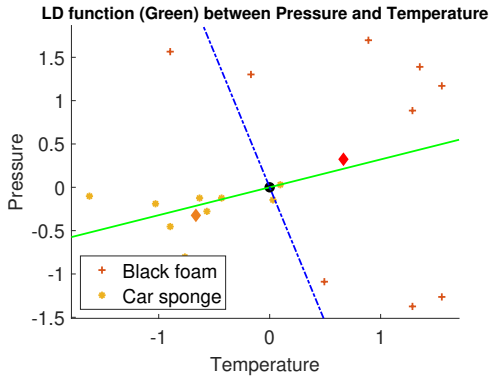

Figure 22: LD function (green) for the pressure and temperature feature space of the black foam and car sponge. The separating hyperplane (line) is shown in blue.

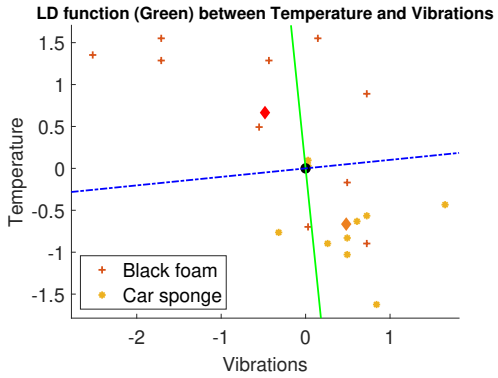

Figure 23: LD function (green) for the temperature and vibrations feature space of the black foam and car sponge. The separating hyperplane (line) is shown in blue.

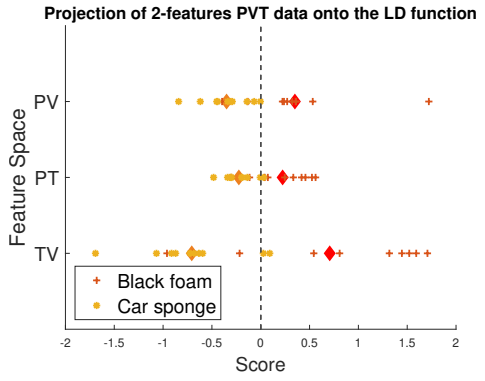

Figure 24: Projection of the black foam and car sponge PVT data onto the LD functions associated with the feature space defined by the y-axis (e.g. PV: pressure and vibrations feature space)

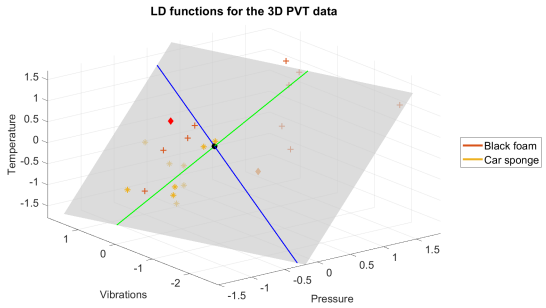

Figure 25: Two LD functions (green and blue) with the largest eigenvalues for the black foam and car sponge 3D PVT data. The plane defined by the two LD functions is shown in gray.

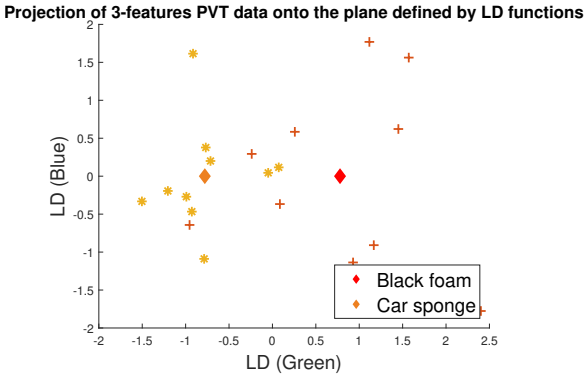

Figure 26: Projection of the black foam and car sponge PVT data onto the space defined by the two LD functions with the largest eigenvalues

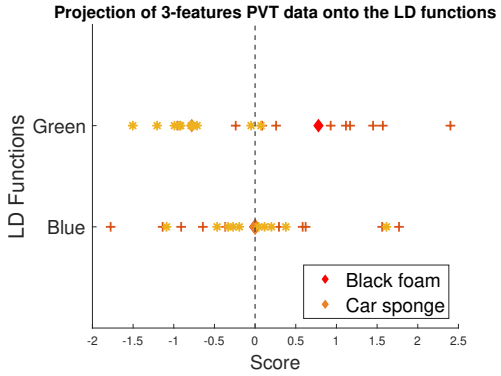

Figure 27: Projection of the black foam and car sponge PVT data onto the two LD functions with the largest eigenvalues

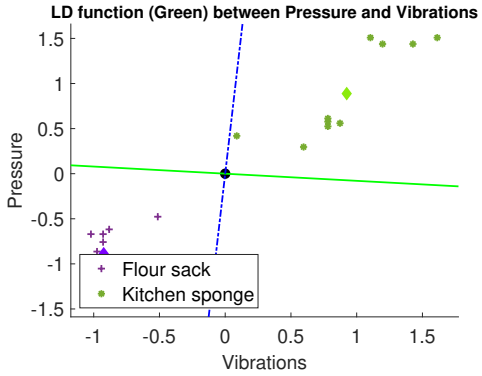

Figure 28: LD function (green) for the pressure and vibrations feature space of the flour sack and kitchen sponge. The separating hyperplane (line) is shown in blue.

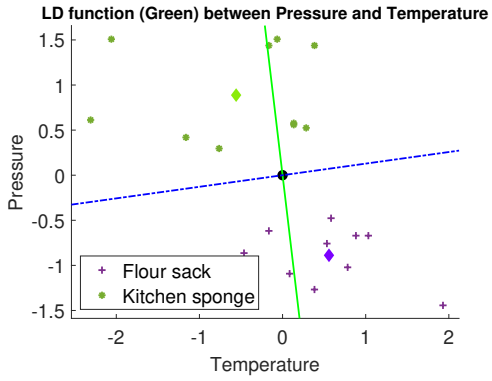

Figure 29: LD function (green) for the pressure and temperature feature space of the flour sack and kitchen sponge. The separating hyperplane (line) is shown in blue.

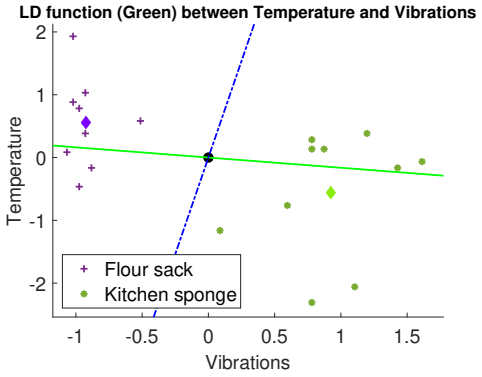

Figure 30: LD function (green) for the tempearture and vibrations feature space of the flour sack and kitchen sponge. The separating hyperplane (line) is shown in blue.

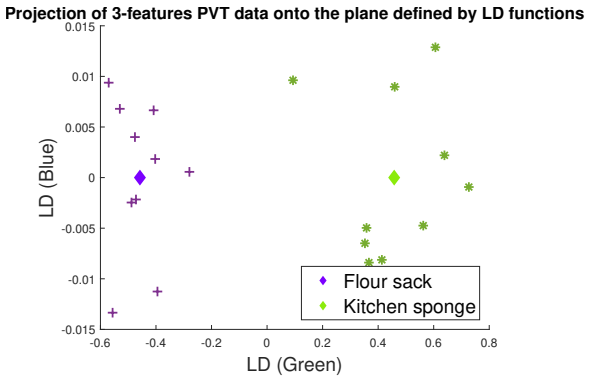

Figure 33: Projection of the flour sack and kitchen sponge PVT data onto the space defined by the two LD functions with the largest eigenvalues

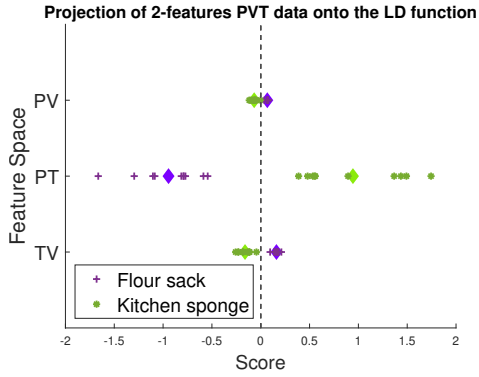

Figure 31: Projection of the flour sack and kitchen sponge PVT data onto the LD functions associated with the feature space defined by the y-axis (e.g. PV: pressure and vibrations feature space)

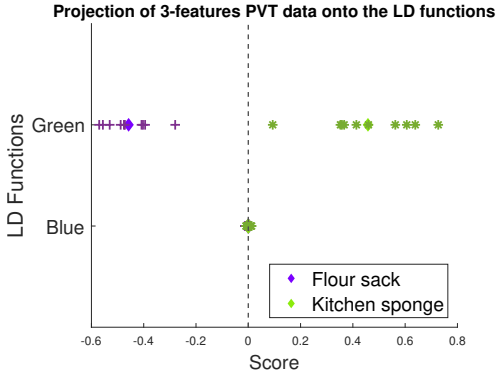

Figure 34: Projection of the flour sack and kitchen sponge PVT data onto the two LD functions with the largest eigenvalues

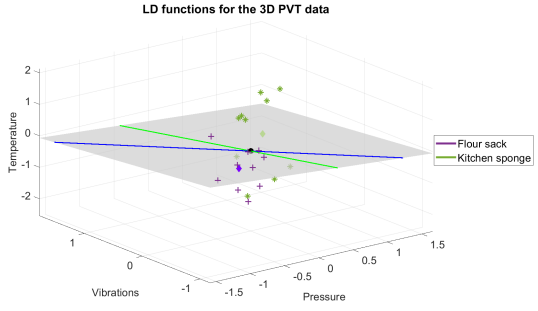

Figure 32: Two LD functions (green and blue) with the largest eigenvalues for the flour sack and kitchen sponge 3D PVT data. The plane defined by the two LD functions is shown in gray.

Appendix D

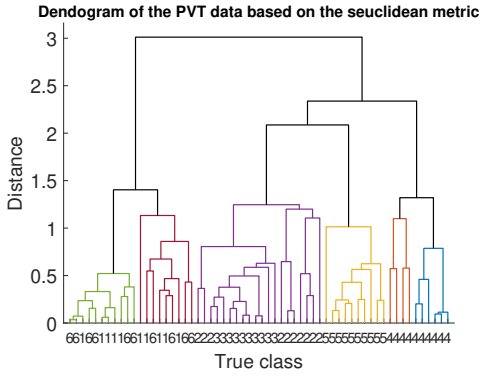

Figure 35: Dendogram of the PVT data based on the *seuclidean* metric

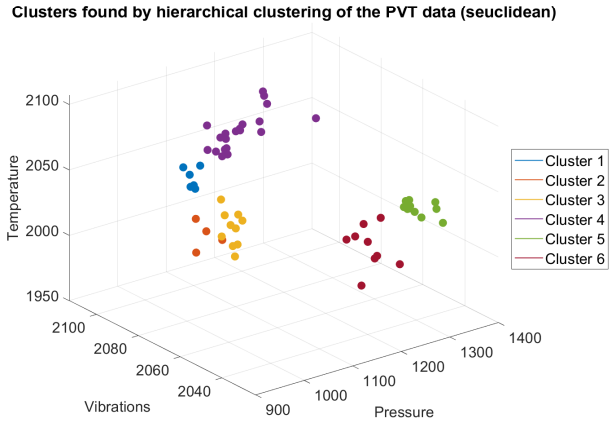

Figure 36: Clusters found by hierarchical clustering of the PVT data based on the *seuclidean* metric

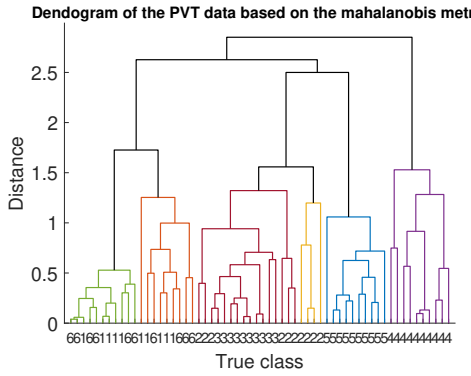

Figure 37: Dendogram of the PVT data based on the *mahalanobis* metric

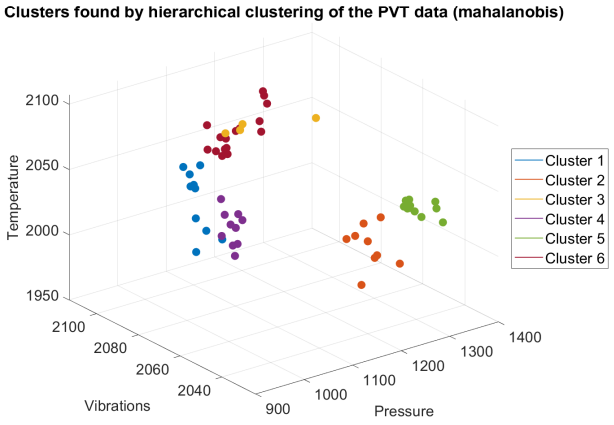

Figure 38: Clusters found by hierarchical clustering of the PVT data based on the *mahalanobis* metric

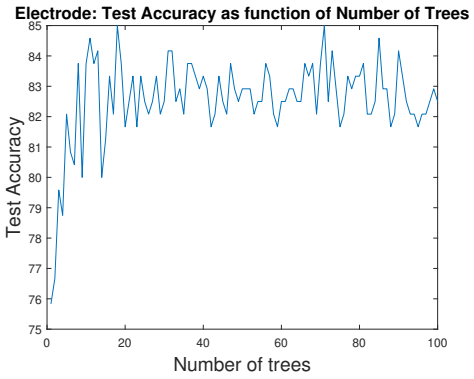

Figure 39: Test classification accuracy against number of trees in the ensemble for the classification of electrode data

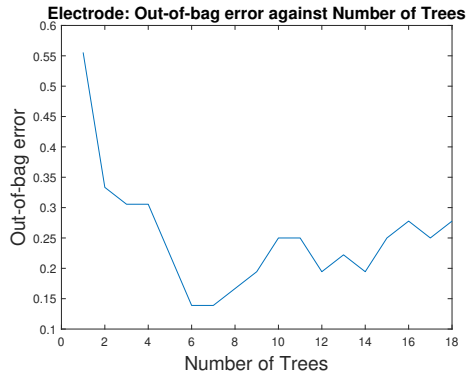

Figure 40: Out-of-bag error against number of trees for classification of electrode data

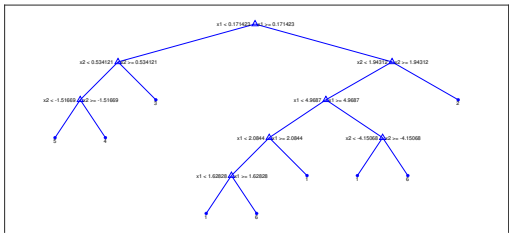

Figure 41: Decision tree 1 in the ensemble of trees for classification of electrode data

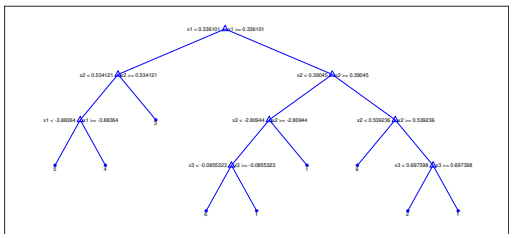

Figure 42: Decision tree 2 in the ensemble of trees for classification of electrode data

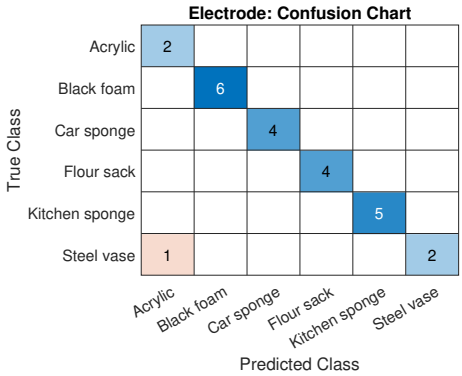

Figure 43: Confusion matrix of the ensemble of 18 trees on the test electrode data